

Production of strange and charmed baryons in pion induced reactions

Sang-Ho Kim,^{1,2,*} Atsushi Hosaka,^{1,3,†} Hyun-Chul Kim,^{1,4,5,‡} and Hiroyuki Noumi^{1,§}

¹*Research Center for Nuclear Physics (RCNP),
Osaka University, Ibaraki, Osaka, 567-0047, Japan*

²*Asia Pacific Center for Theoretical Physics (APCTP),
Pohang, Gyeongbuk, 790-784, Republic of Korea*

³*J-PARC Branch, KEK Theory Center,
Institute of Particle and Nuclear Studies,
KEK, Tokai, Ibaraki, 319-1106, Japan*

⁴*Department of Physics, Inha University,
Incheon 402-751, Republic of Korea*

⁵*School of Physics, Korea Institute for Advanced
Study (KIAS), Seoul 130-722, Republic of Korea*

(Dated: November 30, 2015)

Abstract

We study the strangeness and charm productions induced by the pion beam, i.e. the $\pi^-p \rightarrow K^{*0}\Lambda$ and $\pi^-p \rightarrow D^{*-}\Lambda_c^+$ reactions, based on two different theoretical frameworks: an effective Lagrangian method and a Regge approach. In order to estimate the magnitude of the charm production relative to that of the strangeness production, we assume that the coupling constants for the charmed meson and baryon vertices are the same as those for the strangeness channel. We found that the total cross section for the charm production was about $10^3 - 10^6$ times smaller than that for the strangeness production, depending on theoretical approaches and kinematical regions. We also discuss each contribution to observables for both reactions. In general, the Regge approach explains the experimental data very well over the whole energy region.

PACS numbers: 13.75.Gx, 14.20.Jn, 14.20.Lq, 14.40.Lb

Keywords: strange hadron productions, charmed hadron productions, effective Lagrangian, Regge approach

* E-mail: shkim@rcnp.osaka-u.ac.jp

† E-mail: hosaka@rcnp.osaka-u.ac.jp

‡ E-mail: hchkim@inha.ac.kr

§ E-mail: noumi@rcnp.osaka-u.ac.jp

I. INTRODUCTION

Charm-quark physics becomes one of the most important issues in hadron physics, as experimental facilities report new hadrons containing one or two heavy quarks, either charm quarks or bottom ones, with unprecedented precision. For example, the Belle Collaboration, BABAR Collaboration, and BESIII Collaboration have announced new mesons [1–9], some of which were also confirmed by the LHCb Collaboration [10, 11] (see Refs. [12, 13] for reviews). While the mesons with charm have been extensively studied theoretically as well as experimentally, charmed baryons have been investigated less often. However, the charmed baryons are equally or even more important, since they provide a good opportunity to examine the role of both chiral symmetry and heavy quark symmetry in heavy-light quark systems. Moreover, the structure and the production mechanism of the charmed baryons are much less known than those of light-quark baryons. Recently, a new proposal was submitted at the J-PARC (Japan Proton Accelerator Research Complex) facility for the study of charmed baryons via the pion induced reactions at a high-momentum beam line [14]. There has been only one earlier work at Brookhaven National Laboratory (BNL) almost 30 years ago to search for the charm productions associated with the mechanism $\pi^- p \rightarrow D^{*-} B_c$, where B_c denotes a charmed baryon in ground or excited states [15].

In Ref. [16], the differential cross sections $d\sigma/dt$ for the strangeness and charm productions, i.e. $\pi^- p \rightarrow K^{*0} \Lambda$ and $\pi^- p \rightarrow D^{*-} \Lambda_c^+$, were investigated by using a simple Regge model. As expected, the differential cross section for the charm production was found to be much less than that for the strangeness production. In the present work, we want to further elaborate the previous investigation of these two processes, employing both an effective Lagrangian method and a Regge approach, while putting emphasis on the latter. The effective Lagrangian method has been successfully used to study the production of strangeness hadrons. There are two important ingredients in this method: coupling constants and form factors. The coupling constants are easily determined by using well-known baryon-baryon potentials such as the Nijmegen potential or by considering the experimental data for hadron decays. However, the cutoff masses of the form factors cause ambiguity in describing reactions. In the Regge approach, we also have parameters to fix. In order to determine them, we utilize the quark-gluon string model (QGSM) introduced by Kaidalov *et al* [17–20]. In particular, Ref. [18] studied the $\pi^- p \rightarrow D^- \Lambda_c^+$ reaction within this model, relying only on the D^* reggeon. However, in this work, we consider the contributions of the D and Σ_c reggeons as well as of the D^* reggeon. Before we proceed, we want to shortly mention why we first start with the $D^* \Lambda_c$ production rather than the $D \Lambda_c$ one. The reason lies in the fact that there exists a technical problem in experiment: the background can be reduced more efficiently in reconstructing D^{*-} than in D^- . The decay chain $D^{*-} \rightarrow D^0 + \pi^- \rightarrow K^+ + \pi^- + \pi^-$ allows one to reduce a combinatorial background more effectively.

The present work is organized as follows: In Sec. II, we briefly explain the formalism of the effective Lagrangian method and then present the numerical results of the total cross sections and differential cross sections for pion induced $K^{*0} \Lambda$ and $D^{*-} \Lambda_c^+$ productions. In Sec. III, we derive the transition amplitudes within the Regge approach. We also discuss in this section the results for both the $\pi^- p \rightarrow K^{*0} \Lambda$ and $\pi^- p \rightarrow D^{*-} \Lambda_c^+$ reactions, based on the Regge approach. In Sec. IV, we compare the results from the Regge approach with those from the effective Lagrangian method. We discuss the comparison in detail. The final section is devoted to the summary and the conclusion of the present work.

II. EFFECTIVE LAGRANGIAN APPROACH

In this section, we employ an effective Lagrangian approach to study both the $\pi^- p \rightarrow K^{*0} \Lambda$ and $\pi^- p \rightarrow D^{*-} \Lambda_c^+$ reactions. Starting from the effective Lagrangians describing the interactions between hadrons, we are able to construct the diagrams of t -, s -, and u -channels at the tree level. This effective Lagrangian method has been known to be successful in describing hadron productions near threshold.

A. Lagrangians and Feynman amplitudes

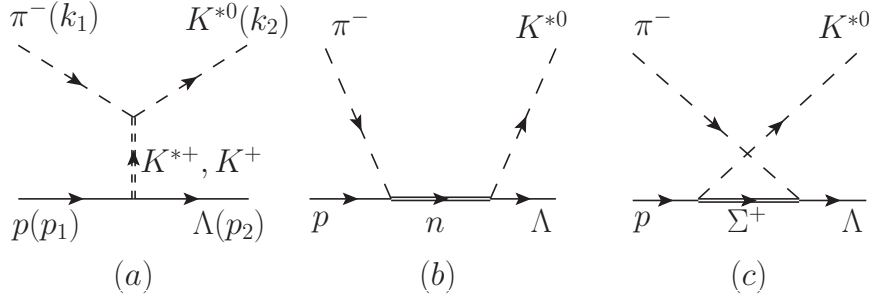


FIG. 1. Tree-level diagrams for $\pi^- p \rightarrow K^{*0} \Lambda$.

We first begin with the $\pi^- p \rightarrow K^{*0} \Lambda$ reaction. The relevant Feynman diagrams are displayed in Fig. 1 in which k_1 and p_1 denote the initial momenta of the π and the proton, respectively. k_2 and p_2 stand for those of the final K^* and Λ , respectively. In this model, we include (a) K and K^* exchanges in the t -channel; (b) the nucleon exchange in the s -channel; and (c) the hyperon (Σ) exchange in the u -channel.

To obtain the invariant Feynman amplitudes, we use the following Lagrangians:

$$\begin{aligned}\mathcal{L}_{\pi K K^*} &= -ig_{\pi K K^*}(\bar{K} \partial^\mu \boldsymbol{\tau} \cdot \boldsymbol{\pi} K_\mu^* - \bar{K}_\mu^* \partial^\mu \boldsymbol{\tau} \cdot \boldsymbol{\pi} K), \\ \mathcal{L}_{\pi K^* K^*} &= g_{\pi K^* K^*} \epsilon^{\mu\nu\alpha\beta} \partial_\mu \bar{K}_\nu^* \boldsymbol{\tau} \cdot \boldsymbol{\pi} \partial_\alpha K_\beta^*,\end{aligned}\tag{1}$$

for the K^* meson and pseudoscalar-octet-meson interactions, where π , K , and K^* designate the fields of $\pi(140, 0^-)$, $K(494, 0^-)$, and $K^*(892, 1^-)$ mesons, respectively. The coupling constant $g_{\pi K K^*}$ is determined by the experimental data of the decay width $\Gamma(K^* \rightarrow K\pi)$ [21]. The decay width is expressed in terms of the coupling constant

$$\Gamma(K^* \rightarrow K\pi) = g_{K^* K \pi}^2 \frac{k_\pi^3}{8\pi M_{K^*}^2},\tag{2}$$

where k_π is the three-momentum of the decaying particle

$$k_\pi = \frac{\sqrt{[M_{K^*}^2 - (M_K + M_\pi)^2][M_{K^*}^2 - (M_K - M_\pi)^2]}}{2M_{K^*}},\tag{3}$$

so that one finds $g_{\pi K K^*} = 6.56$. To determine the $\pi K^* K^*$ coupling constant $g_{\pi K^* K^*}$, we use the hidden local gauge symmetry [22] and flavor $SU(3)$ symmetry. The value of the $\pi K^* K^*$ coupling constant is obtained as $g_{\pi K^* K^*} = 7.45 \text{ GeV}^{-1}$.

The effective Lagrangians for the pseudoscalar meson and baryon octet vertices are written as

$$\begin{aligned}\mathcal{L}_{\pi NN} &= \frac{g_{\pi NN}}{2M_N} \bar{N} \gamma_\mu \gamma_5 \partial^\mu \boldsymbol{\tau} \cdot \boldsymbol{\pi} N, \\ \mathcal{L}_{\pi \Sigma \Lambda} &= \frac{g_{\pi \Sigma \Lambda}}{M_\Lambda + M_\Sigma} \bar{\Lambda} \gamma_\mu \gamma_5 \partial^\mu \boldsymbol{\pi} \cdot \boldsymbol{\Sigma} + \text{H.c.}, \\ \mathcal{L}_{K N \Lambda} &= \frac{g_{K N \Lambda}}{M_N + M_\Lambda} \bar{N} \gamma_\mu \gamma_5 \Lambda \partial^\mu K + \text{H.c.}\end{aligned}\quad (4)$$

where N , Λ , and Σ , denote the nucleon, $\Lambda(1116)$, and $\Sigma(1190)$ baryon fields, respectively. The values of the coupling constants $g_{\pi NN} = 13.3$, $g_{\pi \Sigma \Lambda} = 11.9$, and $g_{K N \Lambda} = -13.4$ are taken from the Nijmegen soft-core model (NSC97a) [23].

The interaction between the K^* vector meson and the baryon octet is described by the following effective Lagrangian

$$\mathcal{L}_{K^* N Y} = -g_{K^* N Y} \bar{N} \left[\gamma_\mu Y - \frac{\kappa_{K^* N Y}}{M_N + M_Y} \sigma_{\mu\nu} Y \partial^\nu \right] K^{*\mu} + \text{H.c.}, \quad (5)$$

where Y generically stands for Λ or $\boldsymbol{\tau} \cdot \boldsymbol{\Sigma}$. We again take the values of the coupling constants $g_{K^* N Y}$ and $\kappa_{K^* N Y}$ from the Nijmegen potential [23]

$$\begin{aligned}g_{K^* N \Lambda} &= -4.26, \quad \kappa_{K^* N \Lambda} = 2.91, \\ g_{K^* N \Sigma} &= -2.46, \quad \kappa_{K^* N \Sigma} = -0.529.\end{aligned}\quad (6)$$

The scattering amplitude for the $\pi N \rightarrow K^* \Lambda$ process can be written as

$$\mathcal{M} = \varepsilon_\mu^* \bar{u}_\Lambda \mathcal{M}^\mu u_N, \quad (7)$$

where u_N and u_Λ denote the Dirac spinors for the incoming nucleon and for the outgoing Λ , respectively, and ε_μ stands for the polarization vector of the outgoing K^* meson. The corresponding amplitude to each channel is obtained as follows:

$$\begin{aligned}\mathcal{M}_K^\mu &= I_K \frac{ig_{\pi K K^*}}{t - M_K^2} \frac{g_{K N \Lambda}}{M_N + M_\Lambda} \gamma^\nu \gamma_5 k_1^\mu (k_2 - k_1)_\nu, \\ \mathcal{M}_{K^*}^\mu &= I_{K^*} \frac{g_{\pi K^* K^*} g_{K^* N \Lambda}}{t - M_{K^*}^2} \epsilon^{\mu\nu\alpha\beta} \left[\gamma_\nu - \frac{i\kappa_{K^* N \Lambda}}{M_N + M_\Lambda} \sigma_{\nu\lambda} (k_2 - k_1)^\lambda \right] k_{2\alpha} k_{1\beta}, \\ \mathcal{M}_N^\mu &= I_N \frac{ig_{K^* N \Lambda}}{s - M_N^2} \frac{g_{\pi NN}}{2M_N} \left[\gamma^\mu - \frac{i\kappa_{K^* N \Lambda}}{M_N + M_\Lambda} \sigma^{\mu\nu} k_{2\nu} \right] (\not{k}_1 + \not{p}_1 + M_N) \gamma^\alpha \gamma_5 k_{1\alpha}, \\ \mathcal{M}_\Sigma^\mu &= I_\Sigma \frac{ig_{K^* N \Sigma}}{u - M_\Sigma^2} \frac{g_{\pi \Sigma \Lambda}}{M_\Sigma + M_\Lambda} \gamma^\alpha \gamma_5 (\not{p}_2 - \not{k}_1 + M_\Sigma) \left[\gamma^\mu - \frac{i\kappa_{K^* N \Sigma}}{M_N + M_\Sigma} \sigma^{\mu\nu} k_{2\nu} \right] k_{1\alpha}.\end{aligned}\quad (8)$$

The isospin factors are given as $I_K = I_{K^*} = I_N = I_\Sigma = \sqrt{2}$. With the form factors taken into account, the total result for the invariant amplitude is written as

$$\mathcal{M}(\pi^- p \rightarrow K^{*0} \Lambda) = \mathcal{M}_K \cdot F_K + \mathcal{M}_{K^*} \cdot F_{K^*} + \mathcal{M}_N \cdot F_N + \mathcal{M}_\Sigma \cdot F_\Sigma. \quad (9)$$

We choose the following form of the form factors

$$F_{ex}(p^2) = \frac{\Lambda^4}{\Lambda^4 + (p^2 - M_{ex}^2)^2}, \quad (10)$$

where p and M_{ex} designate generically the transfer momentum and the mass of the exchanged particle, respectively. The cutoff mass Λ is usually fitted to reproduce the experimental data

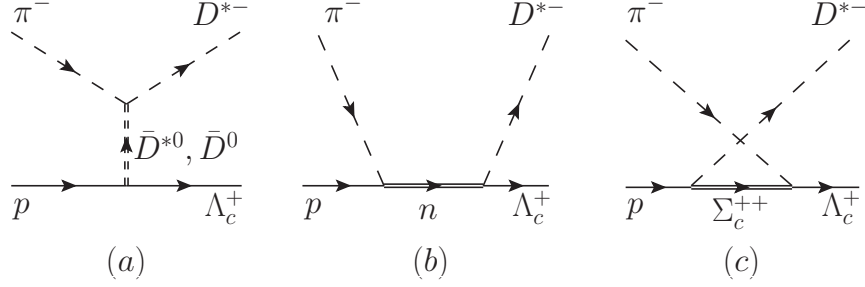


FIG. 2. Tree-level diagrams for $\pi^- p \rightarrow D^{*-} \Lambda_c^+$.

and depends on the reaction channel, K , K^* , N , and Σ -exchanges. However, to minimize the number of parameters for a rough estimation of the production rate, we employ two different cutoff parameters for the meson exchanges and baryon exchanges, separately, which are chosen to be $\Lambda_{K,K^*} = 0.55 \text{ GeV}$ and $\Lambda_{N,\Sigma} = 0.60 \text{ GeV}$.

The Feynman amplitude \mathcal{M} is related to the differential cross section as

$$\frac{d\sigma}{dt} = \frac{1}{64\pi(p_{\text{cm}})^2 s} \frac{1}{2} \sum_{s_i, s_f, \lambda_f} |\mathcal{M}|^2, \quad (11)$$

where s_i and s_f stand for the spins of the nucleon and the Λ , respectively. λ_f denotes the polarization label of the K^* meson and p_{cm} the momentum of the pion in the center-of-mass frame.

Now we turn to the charm production reaction $\pi^- p \rightarrow D^{*-} \Lambda_c^+$. The relevant Feynman diagrams are depicted in Fig. 2. The amplitude for this charm production reaction is obtained just by replacing the strange mesons and hyperons with the charmed ones. In principle, the coupling constants for the charmed hadrons should be different from those for the strange hadrons. In the present calculation, however, we use the same strengths for the corresponding vertices when the coupling constants are dimensionless. This might be considered to be a good assumption if strange and charm quarks are sufficiently heavy. On the other hand, for the coupling constant $g_{\pi K^* K^*}$ which carries the dimension of the inverse mass, we introduce the scaling as $g_{\pi D^* D^*} = M_{K^*}/M_{D^*} \cdot g_{\pi K^* K^*}$. In practice, it is known that the coupling constant $g_{\pi D D^*}$ is about twice as large as the $g_{\pi K K^*}$. This difference of the strengths between $g_{\pi D D^*}$ and $g_{\pi K K^*}$ could be the source of the ambiguity in the present calculation, which would influence the magnitude of amplitudes. As for the form factors, we will use the same form as Eq. (10) with the equal cutoff masses. By doing that, we can directly compare the magnitude of the total cross section for the $\pi N \rightarrow D^* \Lambda_c$ reaction with that for the $\pi N \rightarrow K^* \Lambda$.

B. Results for $K^{*0} \Lambda$ production

Let us first show contributions of each channel to the total cross section for the reaction $\pi^- p \rightarrow K^{*0} \Lambda$. In Fig. 3, they are drawn as a function of s/s_{th} , where s_{th} is the value of s at threshold, i.e. $s_{\text{th}} = (m_{K^*} + m_\Lambda)^2 = 4.05 \text{ GeV}^2$. As shown in Fig. 3, the t -channel process makes the most dominant contribution to the total cross section. K exchange plays a crucial role in describing the total cross section in the low-energy region, whereas K^* exchange governs its behavior in the high-energy region. The reason lies in the fact that

the contribution of K exchange decreases as s increases, while the effect of K^* exchange becomes larger than that of K exchange as the value of s/s_{th} becomes greater than around 3. Though the contribution of K^* exchange seems to increase as s increases, it turns out to be almost constant as s becomes very large. In fact, one can show analytically that when s is very large, the total cross section is proportional to s^{J-1} , where J stands for the spin of an exchange particle in the t -channel. This is the reason why K exchange contributes mainly to the low-energy region, whereas K^* exchange comes into play when s/s_{th} gets large. On the other hand, the contribution of baryon exchanges is almost negligible over the whole energy region.

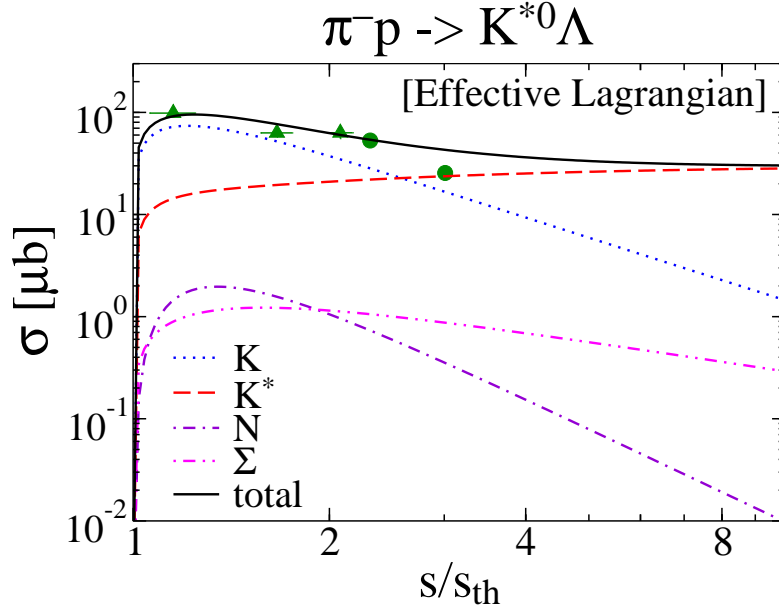


FIG. 3. (Color online). Each contribution to the total cross sections for the $\pi^-p \rightarrow K^{*0}\Lambda$ reaction given as a function of s/s_{th} , based on an effective Lagrangian approach. The dotted and dashed curves show the contributions of K exchange and K^* exchange, respectively. The dot-dashed and dot-dot-dashed ones draw the effects of N and Σ exchanges, respectively. The solid curve represents the total result. The experimental data are taken from Ref. [24] (triangles) and from Ref. [25] (circles).

The result of the total cross section is in good agreement with the experimental data [24, 25] in the relatively low-energy region ($s/s_{\text{th}} \lesssim 2.1$). However, the present result starts to deviate from the experimental data when s/s_{th} reaches the value of around 2.5. Generally, the effective Lagrangian method for the Born approximation at the tree level is a good approximation for the lower-energy regions near threshold, which, however, may not be used at high energies as it often violates the unitarity.

Each contribution to the differential cross section $d\sigma/d\Omega$ for the $\pi^-p \rightarrow K^{*0}\Lambda$ reaction is illustrated in Fig. 4 as a function of $\cos\theta$ at three different momenta, i.e. $P_{\text{lab}} = 3.0 \text{ GeV}/c$, $4.5 \text{ GeV}/c$, and $6.0 \text{ GeV}/c$. Note that the experimental data exist only for $P_{\text{lab}} = 4.5 \text{ GeV}/c$. The θ is the scattering angle between the incoming π and the outgoing K^* meson in the center-of-mass frame. As shown in Fig. 4, K and K^* exchanges make similar contributions to $d\sigma/d\Omega$: Their effects diminish as $\cos\theta$ decreases except that the contribution of K^* exchange is sharply reduced at the very forward angle. While N exchange makes only a minor

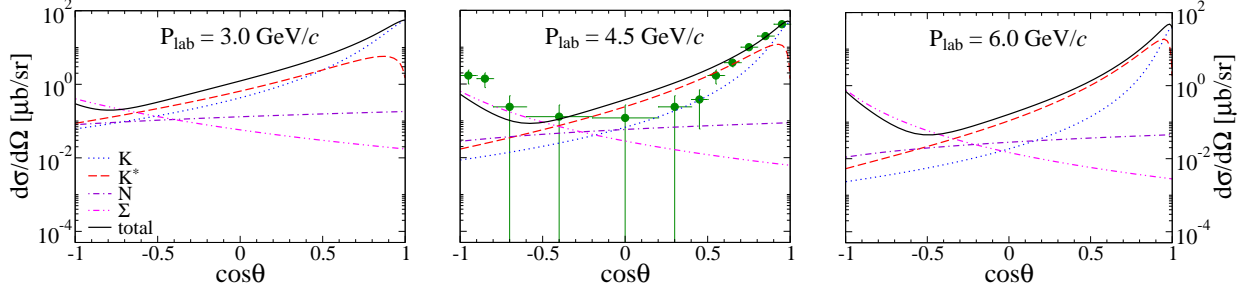


FIG. 4. (Color online). Differential cross sections for the $\pi^-p \rightarrow K^{*0}\Lambda$ reaction as functions of $\cos\theta$ at three different pion momenta (P_{lab}), based on an effective Lagrangian approach. The experimental data are taken from Ref. [25]. The notations are the same as Fig. 3.

contribution, Σ exchange in the u -channel becomes dominant at the very backward angles. As P_{lab} increases, the K -exchange contribution diminishes faster with $\cos\theta$ decreased. On the other hand, the u -channel contribution reveals behavior opposite to the t -channel ones. Because of these different characters of each contribution, the dip structure appearing in the differential cross section becomes deeper as P_{lab} increases.

The t -channel contribution explains the experimental data [25] very well in the forward direction at $P_{\text{lab}} = 4.5 \text{ GeV}/c$, while they start to deviate from the data, as $\cos\theta$ decreases. The result is underestimated at the backward angles. Moreover, if one takes a close look at the experimental data, one finds that $d\sigma/d\Omega$ turns flat between $\cos\theta = 0.3$ and $\cos\theta = -0.7$. The dip structure that the effective Lagrangian method produces is not enough to describe this flatness at intermediate angles. We will discuss this structure in more detail later within the Regge approach.

Figure 5 shows the results of the differential cross sections $d\sigma/dt$ for the $\pi^-p \rightarrow K^{*0}\Lambda$ reaction at four different momenta $P_{\text{lab}} = 3.93 \text{ GeV}/c$, $3.95 \text{ GeV}/c$, $4.5 \text{ GeV}/c$, and $6.0 \text{ GeV}/c$, compared with the experimental data. They are drawn as functions of $-t' = t_{\text{max}} - t$, where the minimum and maximum values of t are given kinematically as

$$t_{\text{min}}^{\text{max}} = M_{\pi}^2 + M_{K^*}^2 - \frac{1}{2s} \left[[s - (M_N^2 - M_{\pi}^2)][s - (M_{\Lambda}^2 - M_{K^*}^2)] \right. \\ \left. \mp \sqrt{[s - (M_N + M_{\pi})^2][s - (M_N - M_{\pi})^2]} \right] \\ \sqrt{[s - (M_{\Lambda} + M_{K^*})^2][s - (M_{\Lambda} - M_{K^*})^2]} \Bigg], \quad (12)$$

respectively. For each of the fixed energies, t varies between t_{min} and t_{max} (or $-t'$ varies between 0 and $t_{\text{max}} - t_{\text{min}}$). The contributions of the t -channel decrease as $-t'$ increases, as expected. K exchange governs $d\sigma/dt$ near $-t' \approx 0$, whereas K^* exchange becomes the main contribution to $d\sigma/dt$. This feature does not change in general, even though P_{lab} increases. The s - and u -channels are negligible. The results from the effective Lagrangian approach are in good agreement with the experimental data between $-t' = 0$ and $-t' = 1.2 \text{ GeV}^2$, but start to deviate from the data as $-t'$ increases. Note that the effective Lagrangian method can only explain the data in the smaller $-t'$ region when $P_{\text{lab}} = 6.0 \text{ GeV}/c$.

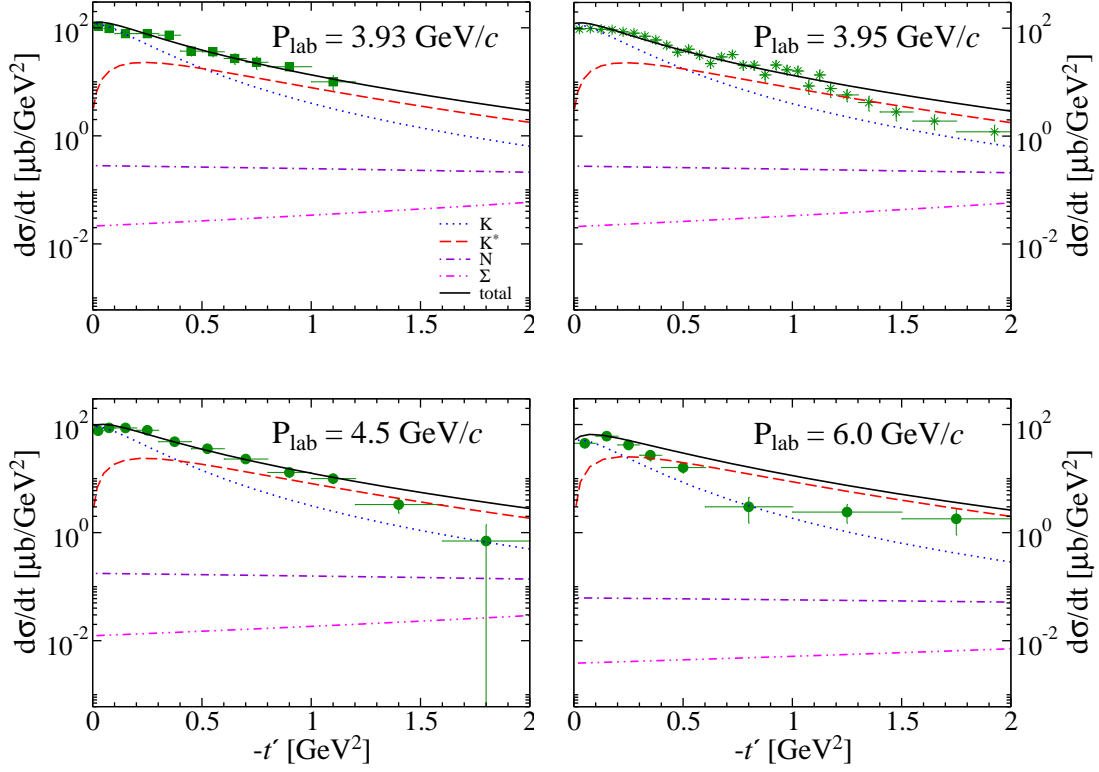


FIG. 5. (Color online). Differential cross sections for the $\pi^-p \rightarrow K^{*0}\Lambda$ reaction as functions of $-t'$ at four different pion momenta (P_{lab}), based on an effective Lagrangian approach. The experimental data denoted by the squares are taken from Ref. [26], and those denoted by the stars from Ref. [27]. Those designated by the circles are taken from Ref. [25]. The notations are the same as Fig. 3.

C. Results for $D^{*-}\Lambda_c^+$ production

We now turn to the charm production. In the left panel of Fig. 6, the results of the total cross section as well as various contributions for the $\pi^-p \rightarrow D^{*-}\Lambda_c^+$ reaction are drawn as a function of s/s_{th} . Note that s_{th} is different from the case of strangeness production, i.e. $s_{\text{th}} = (m_{D^*} + m_{\Lambda_c})^2 = 18.4 \text{ GeV}^2$. In contrast with the $K^*\Lambda$ production, the effect of D exchange is very much suppressed in the $D^*\Lambda_c$ production, while D^* exchange dominates the process, as shown in the left panel of Fig. 6. As mentioned in the case of the strangeness production, the total cross section for the $\pi N \rightarrow D^*\Lambda_c$ reaction is proportional to s^{J-1} when s is large, so that D^* exchange dictates the total cross section at higher energies. All other contributions including D exchange have some effects on it only in the vicinity of threshold. The result of the total cross section for the $\pi^-p \rightarrow D^{*-}\Lambda_c^+$ reaction is compared with that for the $\pi^-p \rightarrow K^{*0}\Lambda$ in the right panel of Fig. 6. The total cross section for the charm production is about 10^4 times smaller than that for the strangeness one near the threshold region and is about 10^3 times smaller at around $s/s_{\text{th}} = 10$. It turns out that, in the effective Lagrangian method, this suppression is mostly caused by the effect of form factors.

The difference in the differential cross section $d\sigma/d\Omega$ is also analyzed in Fig 7. As expected from the result of the total cross section, D^* exchange is dominant, particularly in the range

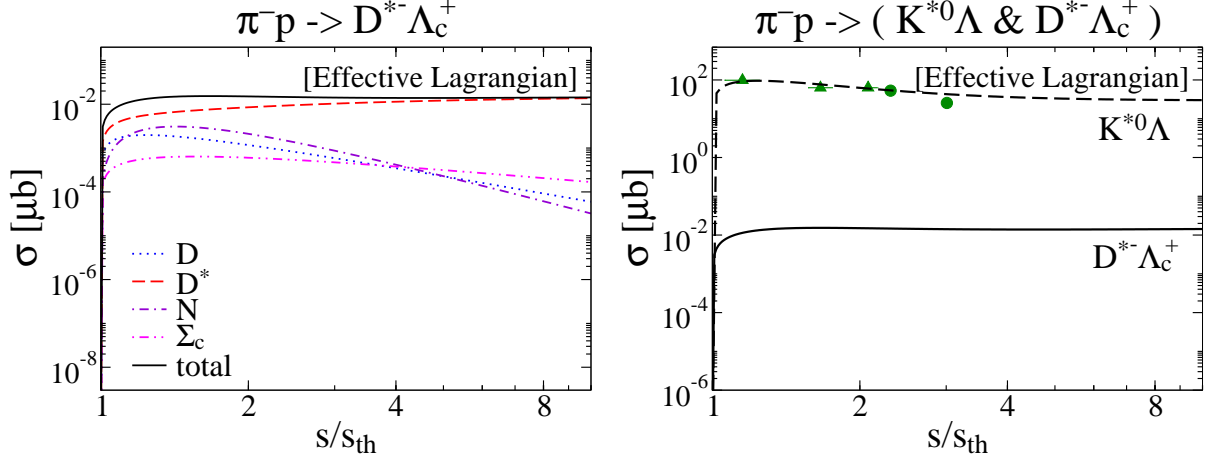


FIG. 6. (Color online). In the left panel, each contribution to the total cross sections for the $\pi^- p \rightarrow D^{*-} \Lambda_c^+$ reaction is drawn as a function of s/s_{th} from an effective Lagrangian approach. The dotted and dashed curves show t -channel contributions, i.e. those of D exchange and D^* exchange, respectively. The dot-dashed and dot-dot-dashed ones depict the contributions of baryon exchange (N and Σ_c), respectively. The solid curve represents the full result of the total cross section. In the right panel, the total cross section for the $\pi^- p \rightarrow D^{*-} \Lambda_c^+$ reaction (solid curve) is compared with that for the $\pi^- p \rightarrow K^{*0} \Lambda$ one (dashed one). The experimental data for the $\pi^- p \rightarrow K^{*0} \Lambda$ reaction are taken from Ref. [24] (triangles) and from Ref. [25] (circles).

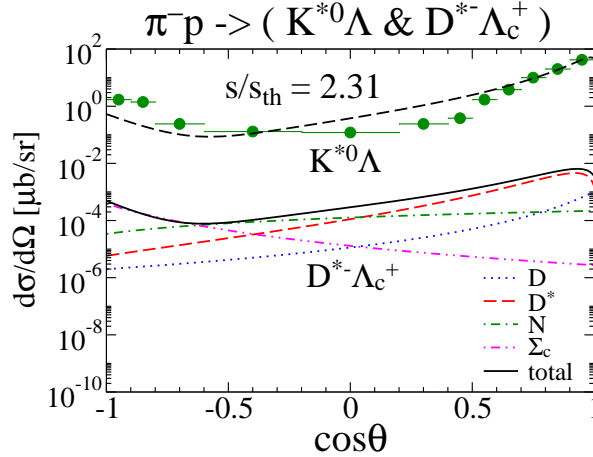


FIG. 7. Comparison of the differential cross section for the $\pi^- p \rightarrow D^{*-} \Lambda_c^+$ with that for the $\pi^- p \rightarrow K^{*0} \Lambda$ based on an effective Lagrangian approach. The experimental data are taken from Ref. [25].

of $0 \leq \cos\theta \leq 1$. In the backward region, Σ_c exchange governs the charm process.

III. REGGE APPROACH

Spurred on by the finding that the effective Lagrangian method describes experimental data mainly in lower-energy regions in the previous section, we will introduce in this sec-

tion a Regge approach, which is known to explain very well high-energy scattering with unitarity preserved. The relevant diagrams for the strangeness production can be schematically depicted in Fig. 8 by the quark lines. There are two different classes of diagrams: a planar diagram [Fig. 8(a)] and a nonplanar diagram [Fig. 8(b)]. In the Regge theory, the planar diagram is described by reggeon exchange in the t -channel, whereas the nonplanar one corresponds to reggeon exchange in the u -channel.

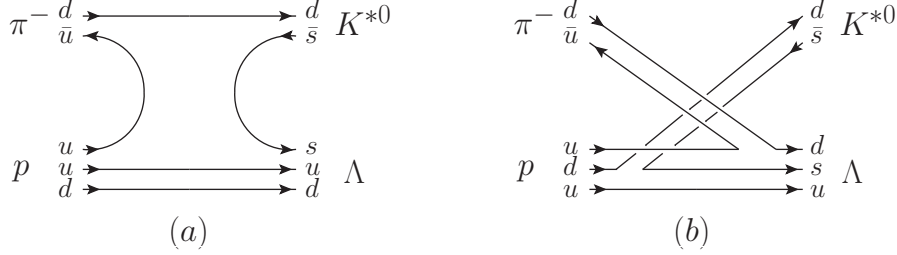


FIG. 8. Planar and nonplanar diagrams for the $\pi^- p \rightarrow K^{*0} \Lambda$ process in the left and right panels, respectively.

A. Regge amplitudes

We first consider the $\pi^- p \rightarrow K^{*0} \Lambda$ reaction. The reggeons in the t -channel are dictated by the K and K^* trajectories, while the Σ -baryon trajectory leads to the reggeon in the u -channel, as displayed in Fig. 8. In the present Regge approach, the Regge amplitudes are derived by replacing the Feynman propagator P^F contained in Eq. (8) by the Regge propagator P^R [28],

$$\begin{aligned} P_K^R(s, t) &= \left(\frac{1}{e^{-i\pi\alpha_K(t)}} \right) \left(\frac{s}{s_K} \right)^{\alpha_K(t)} \Gamma[-\alpha_K(t)] \alpha'_K, \\ P_{K^*}^R(s, t) &= \left(\frac{1}{e^{-i\pi\alpha_{K^*}(t)}} \right) \left(\frac{s}{s_{K^*}} \right)^{\alpha_{K^*}(t)-1} \Gamma[1 - \alpha_{K^*}(t)] \alpha'_{K^*}, \\ P_\Sigma^R(s, u) &= \left(\frac{1}{e^{-i\pi\alpha_\Sigma(u)}} \right) \left(\frac{s}{s_\Sigma} \right)^{\alpha_\Sigma(u)-\frac{1}{2}} \Gamma\left[\frac{1}{2} - \alpha_\Sigma(u)\right] \alpha'_\Sigma, \end{aligned} \quad (13)$$

where $\alpha_K(t)$, $\alpha_{K^*}(t)$, and $\alpha_\Sigma(u)$ denote the Regge trajectories for the K and K^* mesons, and the Σ baryon, respectively. s_K , s_{K^*} , and s_Σ stand for the energy scale parameters for the corresponding reggeons. Thus the Regge amplitudes are represented by

$$\begin{aligned} T_K(s, t) &= \mathcal{M}_K(s, t) P_K^R(s, t) / P_K^F(t), \\ T_{K^*}(s, t) &= \mathcal{M}_{K^*}(s, t) P_{K^*}^R(s, t) / P_{K^*}^F(t), \\ T_\Sigma(s, u) &= \mathcal{M}_\Sigma(s, u) P_\Sigma^R(s, u) / P_\Sigma^F(u), \end{aligned} \quad (14)$$

where \mathcal{M}_K , \mathcal{M}_{K^*} and \mathcal{M}_Σ are the invariant Feynman amplitudes for the K , K^* , and Σ exchanges, respectively, as in Eq. (8) (and form factors are not included here).

The Regge trajectories for K and K^* are taken from Ref. [29], respectively, as $\alpha_K(t) = -0.151 + 0.617t$, $\alpha_{K^*}(t) = 0.414 + 0.707t$. The energy scale parameters are determined by using the QGSM [17–20]: $s_K = 1.752$ and $s_{K^*} = 1.662$. In general, a Regge propagator is

expressed in terms of a linear combination of the two different signatures. However, when a Regge trajectory for a hadron with even spins is approximately the same as that for a hadron with odd spins, that is, the two trajectories are almost degenerate, one of the signatures is canceled out. As displayed in the left panel of Fig. 9, which is taken from Ref. [29], both the K trajectory and the K^* one are almost degenerate. Thus the Regge propagator can have either the signature 1 or $e^{-i\pi\alpha_K(K^*)}$ as shown in Eq. (13) [30, 31].

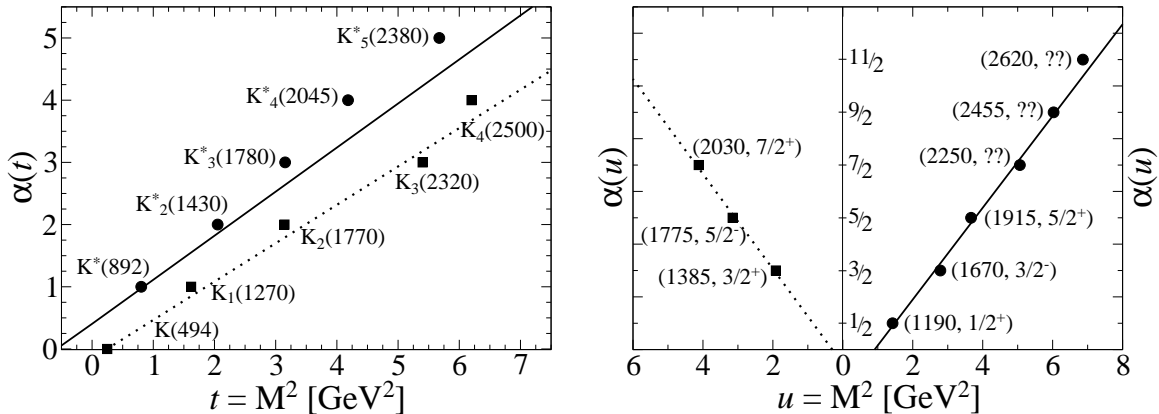


FIG. 9. K and K^* meson trajectories [29] (left panel) and Σ and Σ^* trajectories [32] (right panel).

As for the Σ trajectory, it is not easy to find some tendency like the K and K^* trajectories. In the right panel of Fig. 9, we depict two trajectories for Σ s, assuming that the quantum numbers for some unknown resonances are fixed [32]. In the present calculation, the solid trajectory is taken into account, for which $\alpha_\Sigma(u) = -0.79 + 0.87u$ [32], since it contains the lowest-lying $\Sigma(1190)$. Based on this trajectory, we are able to determine the scale parameter to be $s_\Sigma = 1.569$ by using the QSGM. We also assume that the Σ trajectory is degenerated and two different signatures 1 and $e^{-i\pi\alpha_\Sigma(u)}$ are considered as we did in the mesonic cases.

Since two different signatures are possible for each of reggeon exchanges, there are eight different ways of selecting the signatures for the K , K^* , and Σ Regge propagators. We have examined all the cases and have found that only the low-energy region ($1 \leq s/s_{\text{th}} \leq 2$) is affected by the change in the phases by about 20%. In the present calculation, we choose the signature factor 1 in common for all the Regge propagators.

A unique feature of the Regge amplitudes is that they can reproduce the diffractive pattern both at forward and backward scatterings as well as the asymptotic behavior consistently with the unitarity. Within the framework of a Regge approach, the differential cross sections, $d\sigma/dt$ and $d\sigma/du$, must comply with the following forms asymptotically

$$\frac{d\sigma}{dt}(s \rightarrow \infty, t \rightarrow 0) \propto s^{2\alpha(t)-2}, \quad \frac{d\sigma}{du}(s \rightarrow \infty, u \rightarrow 0) \propto s^{2\alpha(u)-2}. \quad (15)$$

Moreover, the present Regge amplitudes interpolate the low-energy behavior near the threshold region and the high-energy (asymptotic) behavior.

B. Normalization of Regge amplitudes

In many high-energy processes, the absolute values of cross sections are determined empirically. For the effective Lagrangian method, this can be done by employing a form factor.

In the case of the Regge approach, this may be done by considering an overall normalization factor. In addition, some residual t dependence is also included. To fix the undetermined parameters, let us first examine the s dependence of the total cross section and then the t dependence of the differential cross section when taking into account each of the reggeon exchanges separately in comparison with the experimental data for the $K^*\Lambda$ production.

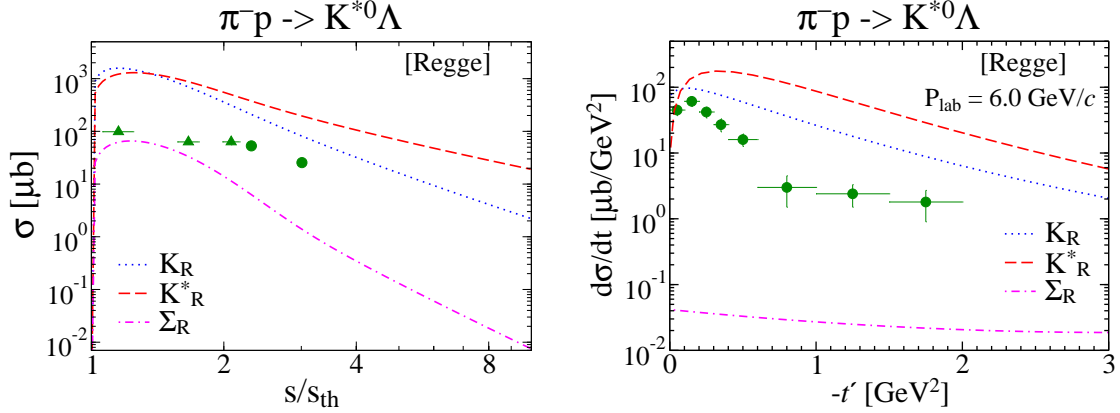


FIG. 10. (Color online) Total cross sections for the $\pi^- p \rightarrow K^{*0} \Lambda$ based on the Regge approach without form factors. The data are taken from Ref. [24] (triangles) and Ref. [25] (circles).

In the left panel of Fig. 10, the total cross section given in Eq. (14) is shown, with each reggeon contribution separately drawn. To start with, let us take a look at the energy dependence while the absolute values will be fixed later. We observe that the K^* reggeon term is in better agreement with the data. The contributions of the K and Σ reggeons fall off faster than the K^* one, because of their smaller values of the intercept $\alpha(0)$. This implies that the K^* reggeon may play a dominant role among the three reggeon contributions. Shown in the right panel of Fig. 10 is the differential cross section $d\sigma/dt$ as a function of $-t'$ at $P_{\text{lab}} = 6.0 \text{ GeV}/c$. At first glance, as $-t'$ is increased, both the K^* and K reggeon terms seem to fall off more slowly than the data. However, if we look at the small $|t'|$ region, to reproduce the sharp decrease at the forward angle, the K^* reggeon seems more important, though some contribution of the K reggeon is also required.

To improve the s and t dependence simultaneously, we introduce an additional factor

$$C_{\text{ex}}(p^2) = \frac{a}{(1 - p^2/\Lambda^2)^2}, \quad (16)$$

which reflects a finite hadron size. Here p stands for the transfer momentum of the exchanged particle. The parameters a and Λ denote a dimensionless constant and a cutoff mass in units of GeV, respectively. The parameter a is introduced to fit the magnitude of the amplitude. This residual factor $C_{\text{ex}}(p^2)$ plays the role of the form factor we have introduced in the effective Lagrangian method. As will be shown in the next section, it greatly improves the t dependence of the differential cross section $d\sigma/dt$. Finally, we express the total result for the invariant Regge amplitude as

$$T(\pi^- p \rightarrow K^{*0} \Lambda) = T_K \cdot C_K + T_{K^*} \cdot C_{K^*} + T_\Sigma \cdot C_\Sigma. \quad (17)$$

In the literature [33], a normalization factor $\mathcal{N}(s, t)$ has been introduced to reproduce the large s behavior by removing the extra s and t dependence possibly coming from the

interaction Lagrangian. The normalization factor is defined by

$$\mathcal{N}(s, t) = \frac{A^\infty(s)}{A(s, t)}, \quad A^2(s, t) = \sum_{s_i, s_f, \lambda_f} |\mathcal{M}(s, t)|^2, \quad (18)$$

where $A^\infty(s)$ is the dominant term when $s \rightarrow \infty$. In the present case, however, such a factor is not needed, because the amplitude (17) already satisfies the desired large s -behavior, and moreover the normalization factor (18) removes the favorable t dependence of the differential cross section in the small $-t$ region. In fact, the decreasing behavior of $d\sigma/dt$ for small $-t$ arises from the t -dependent structure of the effective Lagrangian amplitude that is incorporated in the amplitudes (14) and (17).

We can derive the Regge amplitudes for the charm production in a similar way. Replacing the s quarks in Fig. 7 with c quarks, we can draw the quark diagrams for the $\pi^- p \rightarrow D^{*-} \Lambda_c^+$ process similar to Fig. 7. The relevant amplitudes are written as

$$\begin{aligned} T_D(s, t) &= \mathcal{M}_D(s, t) \left(\frac{s}{s_D} \right)^{\alpha_D(t)} \Gamma[-\alpha_D(t)] \frac{\alpha'_D}{P_D^F(t)}, \\ T_{D^*}(s, t) &= \mathcal{M}_{D^*}(s, t) \left(\frac{s}{s_{D^*}} \right)^{\alpha_{D^*}(t)-1} \Gamma[1 - \alpha_{D^*}(t)] \frac{\alpha'_{D^*}}{P_{D^*}^F(t)}, \\ T_{\Sigma_c}(s, u) &= \mathcal{M}_{\Sigma_c}(s, u) \left(\frac{s}{s_{\Sigma_c}} \right)^{\alpha_{\Sigma_c}(u)-\frac{1}{2}} \Gamma\left[\frac{1}{2} - \alpha_{\Sigma_c}(u)\right] \frac{\alpha'_{\Sigma_c}}{P_{\Sigma_c}^F(u)}. \end{aligned} \quad (19)$$

C. Results for $K^{*0} \Lambda$ production

Having established the strategy above, we fix the strengths of the free parameters a and Λ in $C_{\text{ex}}(p^2)$ in Eq. (16) by the following procedures:

- The cutoff masses Λ are chosen to be the typical values: $\Lambda_{K, K^*, \Sigma} = 1.0 \text{ GeV}$.
- The K^* reggeon dominance being known, its strength is determined by the global s and t dependence of the observed $K^* \Lambda$ production cross sections: $a_{K^*} = 0.8$.
- The strength of the K reggeon amplitude is chosen to reproduce the small $|t|$ behavior of $d\sigma/dt$ together with the dominant K^* reggeon contribution: $a_K = 0.6$.
- The Σ reggeon is determined to reproduce the backward peak behavior: $a_\Sigma = 1.5$.

In Fig. 11, the total cross section is illustrated, together with each contribution. K^* reggeon exchange governs its dependence on s . The contribution of K reggeon exchange is smaller than that of K^* reggeon exchange, which becomes clear as s increases. The reason is obvious from the value of $\alpha_K(t)$ mentioned previously: the corresponding intercept is smaller than that for the K^* trajectory and its slope is steeper than that of the K^* one. We have seen in Fig. 3 that the contribution of K^* exchange in the effective Lagrangian method rises slowly as s increases, which results in deviation from the experimental data. On the other hand, K^* reggeon exchange exhibits the s dependence of the total cross section correctly, so that it describes the experimental data much better than K^* exchange in the effective Lagrangian method at higher values of s . It is interesting to see that Σ reggeon exchange in the u -channel contributes to the total cross section approximately by 20% in

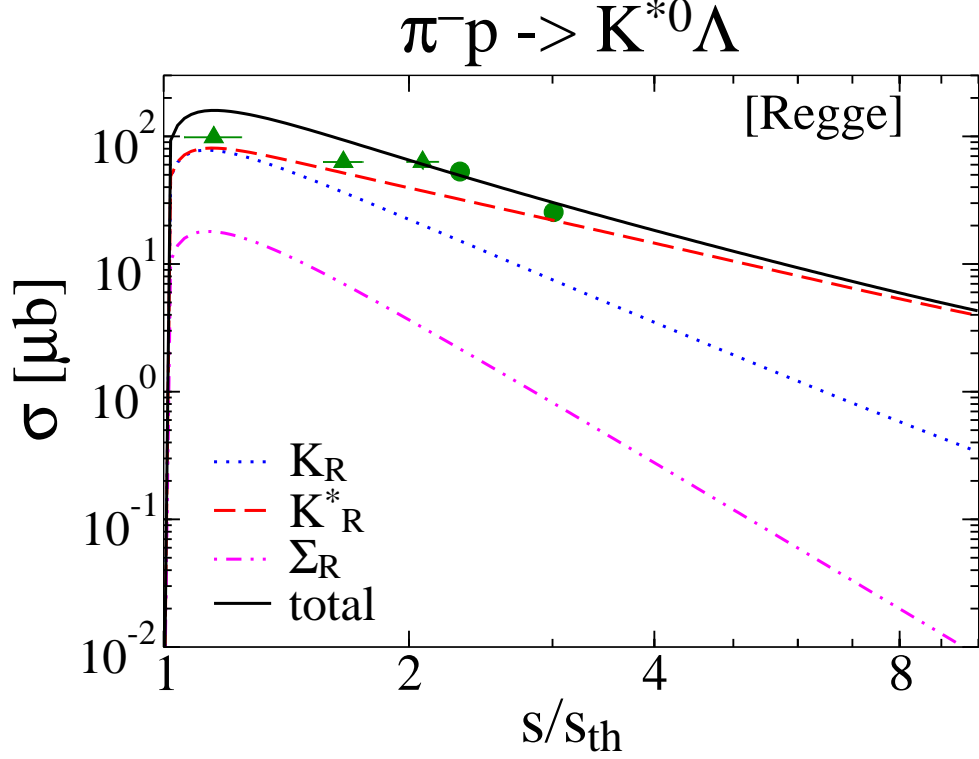


FIG. 11. (Color online). Each contribution to the total cross sections for the $\pi^-p \rightarrow K^{*0}\Lambda$ reaction given as a function of s/s_{th} , based on a Regge approach. The dotted and dashed curves show the contributions of K reggeon exchange and K^* reggeon exchange, respectively. The dot-dot-dashed one draws the effect of Σ reggeon exchange. The solid curve represents the total result. The experimental data are taken from Ref. [24] (triangles) and from Ref. [25] (circles).

the vicinity of threshold whereas its effect becomes much smaller as s increases. This can be understood from the behavior of the u -channel Regge amplitude: $T_\Sigma \sim s^{-0.79}$. Note that this feature of Σ reggeon exchange is significantly different from that of Σ exchange in the effective Lagrangian method, where the u -channel makes a negligibly small contribution (see Fig. 3 for comparison).

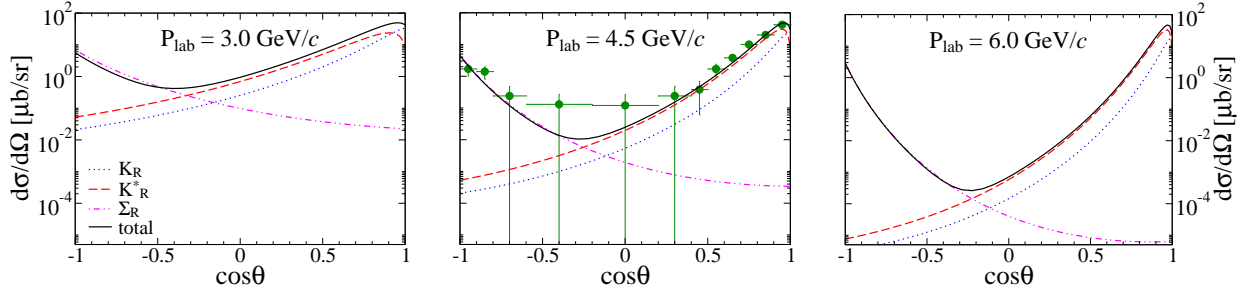


FIG. 12. (Color online). Differential cross sections for the $\pi^-p \rightarrow K^{*0}\Lambda$ reaction as functions of $\cos \theta$ at three different pion momenta (P_{lab}), based on a Regge approach. The experimental data are taken from Ref. [25]. The notations are the same as Fig. 11.

Figure 12 depicts the results of the differential cross section $d\sigma/d\Omega$ for the $\pi^-p \rightarrow K^{*0}\Lambda$ reaction. The K^* reggeon in the t -channel makes a dominant contribution to the differential cross section in the forward region, whereas the Σ reggeon in the u -channel enhances it at the backward angles. The effect of K reggeon exchange is important to describe the experimental data at the very forward angle. We already have found that the results from the effective Lagrangian method deviate from the experimental data except for the forward region. This is to a great extent due to the fact that the u -channel contribution is underestimated in the effective Lagrangian method. However, the Regge approach correctly describes the experimental data at $P_{\text{lab}} = 4.5 \text{ GeV}/c$ over the entire angles. Moreover, on the whole, it elucidates the flatness of the differential cross section between $\cos\theta = 0.3$ and $\cos\theta = -0.7$, which was never explained in the effective Lagrangian method.

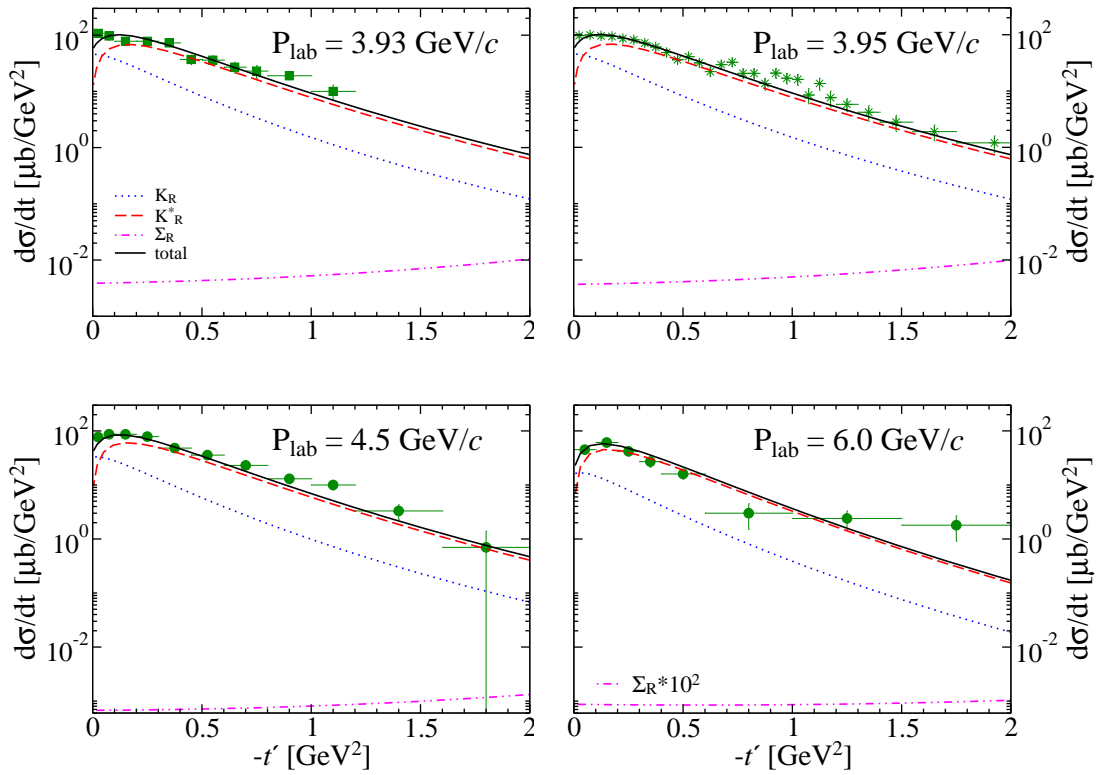


FIG. 13. (Color online). Differential cross sections for the $\pi^-p \rightarrow K^{*0}\Lambda$ reaction as functions of $-t'$ at four different pion momenta (P_{lab}), based on a Regge approach. The experimental data denoted by the squares are taken from Ref. [26], while those denoted by the stars are from Ref. [27]. Those designated by the circles are taken from Ref. [25]. The notations are the same as Fig. 11.

In Fig. 13, we draw the results of the $\pi^-p \rightarrow K^{*0}\Lambda$ differential cross section $d\sigma/dt$ as functions of $-t'$ at four different values of P_{lab} . The most dominant contribution comes from K^* reggeon exchange. K reggeon exchange plays a crucial role in explaining the data at the very forward angle together with K^* reggeon exchange. A similar feature can also be found in the case of $K\Lambda$ photoproduction [30]. The effect of Σ reggeon exchange turns out to be tiny. Though the general feature of the results from the Regge approach looks apparently similar to that of the effective Lagrangian ones, they are in fact different from each other. The results from the Regge approach fall off faster than those from the effective Lagrangian

method, as $-t'$ increases. As a result, the Regge approach reproduces the experimental data better in comparison with the effective Lagrangian method.

D. Results for $D^{*-}\Lambda_c^+$ production

We now discuss the results of the charm production. In the left panel of Fig. 14, we draw the total cross section together with each contribution for the $\pi^- p \rightarrow D^{*-}\Lambda_c^+$ reaction. D^* reggeon exchange dictates the s dependence of the total cross section. The contributions of K reggeon and Σ_c reggeon exchanges are more suppressed than that of K^* reggeon exchange. In the right panel of Fig. 14, we compare the $D^*\Lambda_c$ production with the $K^*\Lambda$ one. It is found that the total cross section for the charm production is approximately $10^4 - 10^6$ times smaller than that for the strangeness production depending on the energy range of s/s_{th} . The resulting production rate for $D^*\Lambda_c$ at $s/s_{\text{th}} \sim 2$, which is the energy that can excite charmed baryons up to ~ 1 GeV, is suppressed by about a factor of 10^4 in comparison with the strangeness production. This implies that the production cross section of $D^*\Lambda_c$ is around 2 nb at that energy.

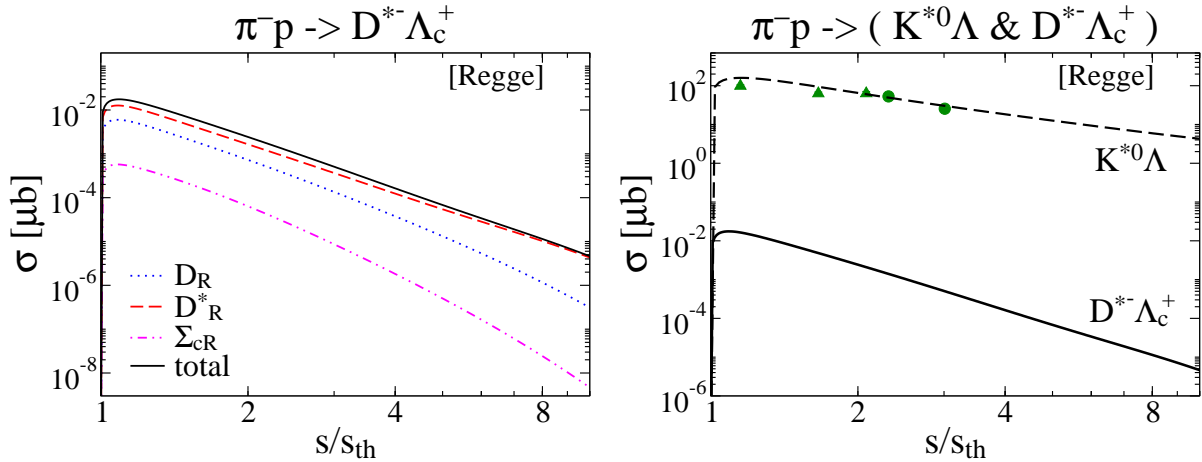


FIG. 14. (Color online). In the left panel, each contribution to the total cross sections for the $\pi^- p \rightarrow D^{*-}\Lambda_c^+$ reaction is drawn as a function of s/s_{th} from a Regge approach. The dotted and dashed curves show t -channel contributions, i.e. those of D reggeon exchange and D^* reggeon exchange, respectively. The dot-dot-dashed curve depicts the contribution of Σ_c reggeon exchange. The solid curve represents the full result of the total cross section. In the right panel, the total cross section for the $\pi^- p \rightarrow D^{*-}\Lambda_c^+$ reaction (solid curve) is compared with that for the $\pi^- p \rightarrow K^{*0}\Lambda$ one (dashed one). The experimental data for the $\pi^- p \rightarrow K^{*0}\Lambda$ reaction are taken from Ref. [24] (triangles) and from Ref. [25] (circles).

In fact, one of the present authors carried out a similar study [34] based on a Regge method from Ref. [35], where a phenomenological form factor was included in the Regge expression for the total cross section. As illustrated in Fig. 3 in Ref. [34], the total cross section for the $D^*\Lambda_c$ production was shown to be approximately 10^4 times smaller than that for the $K^*\Lambda$ production at $s/s_{\text{th}} \sim 2$, which is of almost the same order compared with the present result. However, one has to keep in mind that the form factor introduced by Ref. [35] bears no relation to the effective Lagrangian method. This is understood from the

observation that near the threshold the result of this model is too much underestimated compared with that of the effective Lagrangian method.

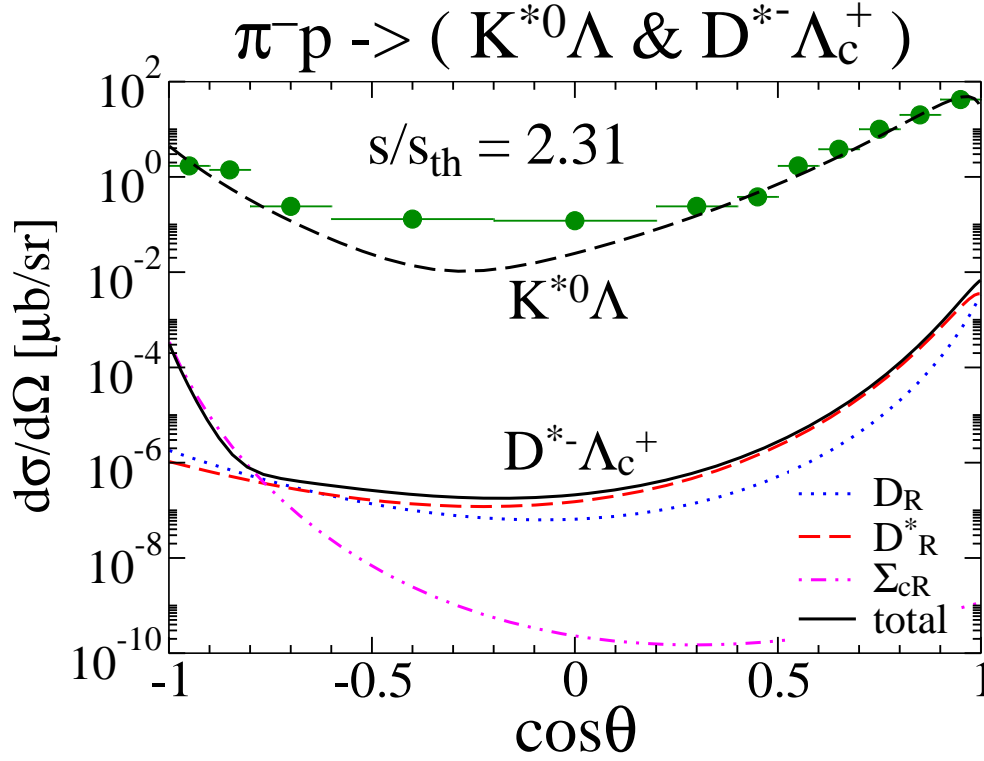


FIG. 15. Comparison of the differential cross section for the $\pi^-p \rightarrow D^{*-}\Lambda_c^+$ with that for the $\pi^-p \rightarrow K^{*0}\Lambda$ based on a Regge approach. The experimental data are taken from Ref. [25].

In Fig. 15, the results of the differential cross section $d\sigma/d\Omega$ for both strangeness and charm productions are also compared to each other. D^* reggeon exchange plays a crucial role throughout the whole angle region. However, its contribution is diminished as $\cos\theta$ decreases, compared with effective Lagrangian method (see Fig. 7).

IV. COMPARISON OF THE TWO MODELS

To analyze what causes the large difference in the cross sections between the strange and charmed productions, we first calculated the cross section without considering form factors. In the effective Lagrangian method, it is interesting that, when excluding the Feynman propagators in Eq. (8) as well as the form factors, each contribution for the charm production is even larger than that for the strangeness one within a factor of 10 except for the N exchange. In the case of N exchange, the difference is between the factors of 10 and 100. Since the energy scale for the charm production is larger than the strangeness one, the Feynman propagator suppresses the charm production much more than the strangeness one. The form factor also contains the $(p^2 - M_{ex}^2)$ term in the denominator which suppresses the amplitude more because it is a second power. However, in the case of the Regge approach, the result of the cross section when excluding form factors is quite different from that of the effective Lagrangian method. The form factors barely affect the difference in the cross sections.

Considering the fact that Ref. [15] has experimentally measured only an upper limit $\sigma \sim 7 \text{ nb}$ at the pion momentum $P_{\text{lab}} = 13 \text{ GeV}/c$ for the charm production, we find that the results derived from our models are within a factor of 2 from this upper limit: $\sigma = 14(9) \text{ nb}$ when employing the effective Lagrangian method (Regge approach). However, some ambiguity lies in the selection of cutoff masses. If we apply slightly smaller cutoff masses, for example, $0.5(0.9) \text{ GeV}$ for the effective Lagrangian method (Regge approach), our results will underestimate the upper limit 7 nb without influencing the general results for the strangeness productions. The slope of the differential cross section also mildly changes with the cutoff masses varied.

V. SUMMARY AND CONCLUSION

In the present work, we aimed at describing both the strangeness and charm productions by the pion beam, based on both an effective Lagrangian method and a Regge approach. We started with the effective Lagrangian method to describe the $\pi N \rightarrow K^* \Lambda$ and $\pi N \rightarrow D^* \Lambda_c$ reactions. The coupling constants were determined either by using the experimental data or by employing those from a nucleon-nucleon potential and flavor SU(3) symmetry. The cutoff masses of the form factors were fixed to reproduce the experimental data. However, in order to reduce the ambiguity in the effective Lagrangian method, we used the equal values of the cutoff masses for each case of meson exchange and baryon exchange.

We were able to explain the total cross section for the $\pi^- p \rightarrow K^{*0} \Lambda$ in lower-energy regions within the framework of the effective Lagrangian method. However, the results from the effective Lagrangian method start to deviate from the data, as the square of the total energy s increases. The magnitude of the total cross section for the $\pi^- p \rightarrow D^{*+} \Lambda_c^+$ was approximately 10^3 times smaller than that for the $\pi N \rightarrow K^* \Lambda$. The t -channel contributes to the differential cross section in the forward direction, whereas the u -channel contributes to that in the backward direction. The differential cross section $d\sigma/dt$ for the $\pi^- p \rightarrow K^{*0} \Lambda$ tends to decrease as $-t'$ increases. The results of $d\sigma/dt$ were in good agreement with the experimental data at lower P_{lab} .

We constructed the Regge propagators for K and K^* reggeons. Since the corresponding trajectories are degenerate, we were able to consider the signature either to be 1 or to be a complex phase. The Σ reggeon was also considered for the description of the backward angle region. We selected 1 as the signatures for all the reggeon propagators. Our Regge model satisfies the asymptotic behavior of the total cross section to a great extent as s becomes very large. The difference between the strange and charmed total cross sections turns out to be $10^4 - 10^6$, depending on the energy range. Compared with the results from the effective Lagrangian method, the Regge approach describes the experimental data better, in particular, in higher-energy regions.

In the present paper, our estimation corresponds to the production rates of the ground state Λ_c associated with a charmed meson D^* . On the other hand, production rates of various excited states together with their decays are related to their structures formed by the heavy- and light-quark contents. The relevance of production rates to different structures of excited states has been addressed previously [16]. The identification of spin doublets, e.g., $J^P = 1/2^-$ and $3/2^-$ states, will clarify the nature of heavy-quark spin symmetry. The identification of different internal modes, the so-called λ and ρ modes [36], can address how two light quarks (diquarks) are excited inside a baryon. The excited diquark may couple to the pion to decay, carrying basic information of chiral symmetry. In future experiments, we

hope to see such fundamental issues of the physics of the strong interaction.

We want to mention that N^* resonances [37, 38] were not considered, because we are mainly interested in higher-energy regions, where the experimental data are available to date. However, it is of great interest to take into account N^* resonances, when one wants to understand the mechanism of the $K^*\Lambda$ production near threshold in detail. In addition, since the K^* meson in the final state is a vector meson, it is very important to understand polarization observables and density matrix elements. Furthermore, we can extend the present work to the reaction $\pi^-p \rightarrow K^{*0}\Sigma^0$ ($K^{*+}\Sigma^-$) and the corresponding charm production $\pi^-p \rightarrow D^{*-}\Sigma_c^+$ ($\bar{D}^{*0}\Sigma_c^0$). The corresponding results will appear elsewhere soon.

ACKNOWLEDGMENTS

This work is supported in part by the Grant-in-Aid for Science Research (C) 26400273. S.H.K. is supported by a Scholarship from the Ministry of Education, Culture, Science and Technology of Japan. The work of H.-Ch.K. was supported by the Basic Science Research Program through the National Research Foundation of Korea funded by the Ministry of Education, Science and Technology (Grant NO. 2013S1A2A2035612).

-
- [1] S. K. Choi *et al.* [Belle Collaboration], Phys. Rev. Lett. **91**, 262001 (2003).
 - [2] B. Aubert *et al.* [BABAR Collaboration], Phys. Rev. D **71**, 071103 (2005).
 - [3] B. Aubert *et al.* [BABAR Collaboration], Phys. Rev. Lett. **95**, 142001 (2005).
 - [4] K. Abe *et al.* [Belle Collaboration], Phys. Rev. Lett. **98**, 082001 (2007).
 - [5] S. K. Choi *et al.* [Belle Collaboration], Phys. Rev. Lett. **100**, 142001 (2008).
 - [6] A. Bondar *et al.* [Belle Collaboration], Phys. Rev. Lett. **108**, 122001 (2012).
 - [7] M. Ablikim *et al.* [BESIII Collaboration], Phys. Rev. Lett. **110**, 252001 (2013).
 - [8] Z. Q. Liu *et al.* [Belle Collaboration], Phys. Rev. Lett. **110**, 252002 (2013).
 - [9] M. Ablikim *et al.* [BESIII Collaboration], Phys. Rev. Lett. **111**, 242001 (2013).
 - [10] R. Aaij *et al.* [LHCb Collaboration], Phys. Rev. Lett. **110**, 222001 (2013).
 - [11] R. Aaij *et al.* [LHCb Collaboration], Phys. Rev. Lett. **112**, 222002 (2014).
 - [12] E. S. Swanson, Phys. Rept. **429**, 243 (2006).
 - [13] N. Brambilla, S. Eidelman, B. K. Heltsley, R. Vogt, G. T. Bodwin, E. Eichten, A. D. Frawley, and A. B. Meyer *et al.*, Eur. Phys. J. C **71**, 1534 (2011).
 - [14] Charmed Baryon Spectroscopy via the (π^-, D^{*-}) reaction (2012). (Available at: http://www.j-parc.jp/researcher/Hadron/en/Proposal_e.html#1301). J-PARC P50 proposal.
 - [15] J. H. Christenson, E. Hummel, G. A. Kreiter, J. Sculli, and P. Yamin, Phys. Rev. Lett. **55**, 154 (1985).
 - [16] S. H. Kim, A. Hosaka, H.-Ch. Kim, H. Noumi, and K. Shirotori, Prog. Theor. Exp. Phys. **2014**, 103D01 (2014).
 - [17] A. B. Kaidalov, Z. Phys. C **12**, 63 (1982).
 - [18] K. G. Boreskov and A. B. Kaidalov, Sov. J. Nucl. Phys. **37**, 100 (1983); [Yad. Fiz. **37**, 174 (1983)].

- [19] A. B. Kaidalov and O. I. Piskunova, Sov. J. Nucl. Phys. **43**, 994 (1986); [Yad. Fiz. **43**, 1545 (1986)].
- [20] A. B. Kaidalov and P. E. Volkovitsky, Z. Phys. C **63**, 517 (1994).
- [21] K. A. Olive *et al.* (Particle Data Group), Chin. Phys. C **38**, 090001 (2014).
- [22] M. Bando, T. Kugo, and K. Yamawaki, Phys. Rept. **164**, 217 (1988).
- [23] V. G. J. Stoks and Th. A. Rijken, Phys. Rev. C **59**, 3009 (1999); Th. A. Rijken, V. G. J. Stoks, and Y. Yamamoto, *ibid.* **59**, 21 (1999).
- [24] O. I. Dahl, L. M. Hardy, R. I. Hess, J. Kirz, and D. H. Miller, Phys. Rev. **163**, 1377 (1967).
- [25] D. J. Crennell, H. A. Gordon, K. -W. Lai, and J. M. Scarr, Phys. Rev. D **6**, 1220 (1972).
- [26] D. Yaffe, M. Abramovich, V. Chaloupka, A. Ferrando, M. Korkea-Aho, M. J. Losty, L. Montanet, E. Paul *et al.*, Nucl. Phys. B **75**, 365, (1974).
- [27] M. Aguilar-Benitez *et al.*, Z. Physik. C, Particles and Fields **6**, 195 (1980).
- [28] A. Donnachie, H. G. Dosch, P. V. Landshoff, and O. Nachtmann, Pomeron Physics and QCD (Cambridge University Press, UK, 2002).
- [29] M. M. Brisudova, L. Burakovsky, and T. Goldman, Phys. Rev. D **61**, 054013 (2000).
- [30] M. Guidal, J. M. Laget, and M. Vanderhaeghen, Nucl. Phys. A **627**, 645 (1997).
- [31] T. Corthals, J. Ryckebusch, and T. Van Cauteren, Phys. Rev. C **73**, 045207 (2006).
- [32] J. K. Storrow, Phys. Rep. **103**, 317 (1984).
- [33] A. I. Titov and B. Kampfer, Phys. Rev. C **78**, 025201 (2008).
- [34] H. Noumi, PoS Hadron **2013**, 031 (2013).
- [35] V. Y. Grishina, L. A. Kondratyuk, W. Cassing, M. Mirazita, and P. Rossi, Eur. Phys. J. A **25**, 141 (2005).
- [36] L. A. Copley, N. Isgur, and G. Karl, Phys. Rev. D **20**, 768 (1979) [Erratum-*ibid.* D **23**, 817 (1981)].
- [37] S. H. Kim, S. i. Nam, Y. Oh, and H.-Ch. Kim, Phys. Rev. D **84**, 114023 (2011).
- [38] S. H. Kim, A. Hosaka, and H.-Ch. Kim, Phys. Rev. D **90**, 014021 (2014).